A novel patch assembly domain in Num1 mediates dynein anchoring at the cortex during spindle positioning

Xianying Tang, Bryan St. Germain, and Wei-Lih Lee

Biology Department, University of Massachusetts Amherst, Amherst, MA 01003

During mitosis in budding yeast, cortically anchored dynein generates pulling forces on astral microtubules to position the mitotic spindle across the mother–bud neck. The attachment molecule Num1 is required for dynein anchoring at the cell membrane, but how Num1 assembles into stationary cortical patches and interacts with dynein is unknown. We show that an N-terminal Bin/Amphiphysin/Rvs (BAR)–like domain in Num1 mediates the assembly of morphologically distinct patches and its interaction with dynein for spindle translocation into the bud. We name this domain patch assembly domain (PA; residues 1–303), as it was both necessary and sufficient for the formation of functional dynein-anchoring patches when it was attached to a pleckstrin homology domain or a CAAX motif. Distinct point mutations targeting the predicted BAR-like PA domain differentially disrupted patch assembly, dynein anchoring, and mitochondrial attachment functions of Num1. We also show that the PA domain is an elongated dimer and discuss the mechanism by which it drives patch assembly.

Introduction

To ensure that cell fate determinants are faithfully distributed to each daughter cell, all dividing eukaryotic cells must correctly position their mitotic spindle with respect to the cleavage plane. During the asymmetric cell division of budding yeast, the mother cell generates a daughter cell through budding at a site of the cell cortex predetermined before mitosis (Chant and Pringle, 1995; Pringle et al., 1995). Segregation of one copy of the genome into the bud requires the mitotic spindle to be aligned along the mother–bud axis, with one spindle pole penetrating into the bud (Shaw et al., 1997; Miller and Rose, 1998; Yeh et al., 2000). In early anaphase, concomitantly with spindle elongation, the nucleus is dragged into the daughter cell through the mother–bud neck, led by the daughter spindle pole moving away from the bud neck (Sullivan and Huffaker, 1992; Yeh et al., 1995; Shaw et al., 1997; Adames and Cooper, 2000). Subsequent cleavage at the narrow mother–bud neck during cytokinesis then divides the bud from the mother, producing two cells of unequal size (Stearns, 1997).

Spindle movement and nuclear migration into the daughter cell depend on the pulling force generated by cytoplasmic dynein between astral microtubules and the bud cortex (Eshel et al., 1993; Li et al., 1993; Carminati and Stearns, 1997; Stearns, 1997; Adames and Cooper, 2000; Yeh et al., 2000). The currently favored model proposes that dynein first tip tracks the distal plus ends of astral microtubules, exploiting the microtubule dynamic instability to probe the bud cortex for attachment sites containing the cortical protein Num1 (Farkasovsky and Küntzel, 1995, 2001; Heil-Chapdelaine et al., 2000; Bloom, 2001; Markus and Lee, 2011b). Upon binding to Num1, dynein becomes anchored at the cortex. Anchored dynein then walks on the astral microtubule toward the minus end by virtue of its motor activity, thereby pulling the nucleus and its associated spindle into the daughter cell (Lee et al., 2003; Sheeman et al., 2003). Cortical force generation by dynein depends on its accessory complex dynactin and is abolished in the absence of the attachment molecule Num1 (McMillan and Tatchell, 1994; Kahana et al., 1998; Adames and Cooper, 2000; Lee et al., 2003; Moore et al., 2008; Markus and Lee, 2011b). Little is known with regard to how Num1 binds and anchors dynein to the cell membrane.

The role of cortically localized dynein in spindle positioning has also been established in various other cell types, including

Correspondence to Wei-Lih Lee: wlee@bio.umass.edu

Abbreviations used in this paper: BAR, Bin/Amphiphysin/Rvs; BiFC, bimolecular fluorescence complementation; HC, heavy chain; HU, hydroxyurea; PH, pleckstrin homology; SPB, spindle pole body; TEV, Tobacco Etch Virus.

The Rockefeller University Press $30.00
J. Cell Biol. Vol. 196 No. 6 743–756
www.jcb.org/cgi/doi/10.1083/jcb.201112017

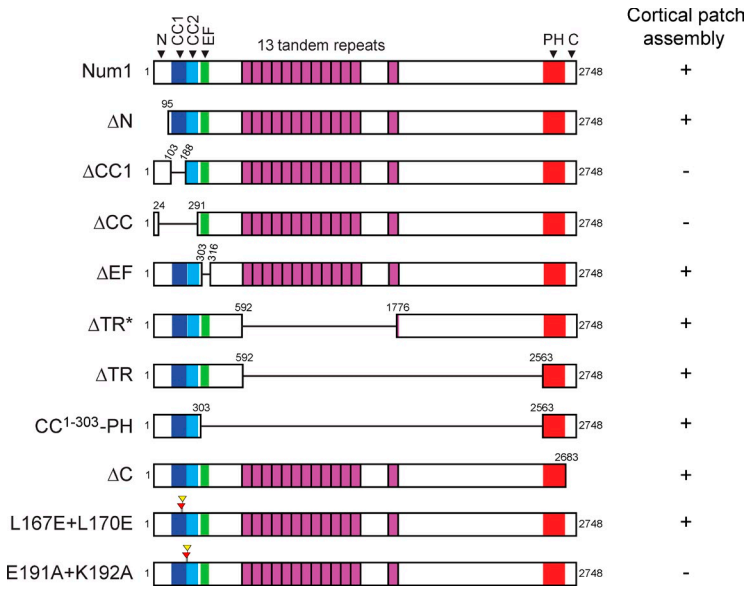

Figure 1. **Num1 constructs in this study.** (Left) Diagram of constructs. Red and yellow triangles indicate locations of point mutations. (right) Plus symbols denote normal patch assembly at the cortex similar to wild-type Num1, and minus symbols denote lack of cortical bright patch or no cortical patch.

Caenorhabditis elegans zygote (Nguyen-Ngoc et al., 2007), *Drosophila melanogaster* neuroblast (Bowman et al., 2006; Siller et al., 2006), HeLa cells (Du and Macara, 2004), and polarized epithelial MDCK cells (Faulkner et al., 2000; Siller and Doe, 2009). Unlike budding yeast, where the only site of action for dynein is at the cell cortex, dynein in these cells performs diverse functions at multiple cellular sites during mitosis. For example, it localizes to the spindle poles for pole focusing (Merdes et al., 2000; Quintyne et al., 2005), to the nuclear envelope during prometaphase to facilitate nuclear envelope breakdown (Salina et al., 2002), and to the kinetochores for spindle assembly checkpoint inactivation (Howell et al., 2001; Wojcik et al., 2001). Very little is known about the spatial regulation of dynein and, in particular, the mechanism of its attachment to the cell cortex. Although recent studies have implicated the heterotrimeric complex NuMA–LGN/G-α_i (Mud/Pins/G-α_i in *Drosophila* and Lin-5/GPR-1/2/G-α_i in *C. elegans*) in mediating cortical dynein localization (Du and Macara, 2004; Bowman et al., 2006; Siller et al., 2006; Nguyen-Ngoc et al., 2007; Woodard et al., 2010), it is still unclear how dynein is captured at the cell membrane for force generation to power spindle movement in these cells (Markus and Lee, 2011a).

To gain insight into the mechanism of cortical anchoring of dynein, we performed a comprehensive structure-function study on Num1. Our work identified a novel domain in Num1 that is required for the assembly of dynein-anchoring sites at the cell cortex. This domain performs dual roles in the dynein-mediated spindle positioning pathway: to assemble Num1 patches at the cell membrane and to mediate physical interaction with the dynein complex. Our biochemical and functional characterizations demonstrate the ability of this domain to self-associate, supporting its role in patch assembly.

Results

Mapping Num1 PA domain

A prominent feature of Num1 is that it forms discrete patches at the cell cortex (Farkasovsky and Küntzel, 1995; Heil-Chapdelaine et al., 2000). This localization requires the C-terminal membrane-targeting pleckstrin homology (PH) domain (Fig. 1; Farkasovsky and Küntzel, 1995; Moore et al., 2009b), which binds phosphoinositide PI(4,5)P_2 with high affinity and specificity (Yu et al., 2004). We previously showed that the sole function of the PH domain is to mediate the recruitment of Num1 to the cortical membrane, and we proposed that an additional step of aggregation, mediated by the sequence N terminal to the PH domain, is required for Num1 to form functional patches (Tang et al., 2009). To identify such sequence, we created a series of Num1 constructs lacking individual domains but retaining the PH domain (Fig. 1). Each mutant was C-terminally tagged with GFP and expressed under the control of the endogenous *NUM1* promoter at the chromosomal locus. We found that all constructs exhibited localization similar to the full-length protein, except those lacking the N-terminal predicted coiled-coil region (Figs. 1 and S1 A).

The coiled-coil region contains two neighboring coiled-coil motifs predicted by the SMART (simple modular architecture research tool) database: CC1, aa 104–187, and CC2, aa 214–290. Deleting CC2 rendered Num1 unstable (Fig. 2 B), hindering further assessment of its effect on localization. Deleting CC1 did not affect protein stability, as immunoblotting detected ΔCC1-GFP at a level similar to Num1-GFP (Fig. 2 B). Interestingly, although ΔCC1-GFP was capable of associating with the cell cortex, it failed to assemble the characteristic bright foci frequently observed for Num1-GFP (Fig. 2, A and C). The mean fluorescence intensity of individual ΔCC1-GFP foci was approximately one third of that of Num1-GFP foci (Fig. 2 D). Furthermore, 96.0% (192 of 200) of ΔCC1-GFP foci had intensities lower than the mean intensity of Num1-GFP foci (Fig. 2 D, blue dashed line). Therefore, we defined patches with brightness above the mean intensity of wild-type Num1-GFP foci as morphologically distinct patches that require the coiled-coil motifs to assemble.

To test whether the coiled-coil motifs are sufficient for patch assembly, we generated a minimal fusion construct composed of

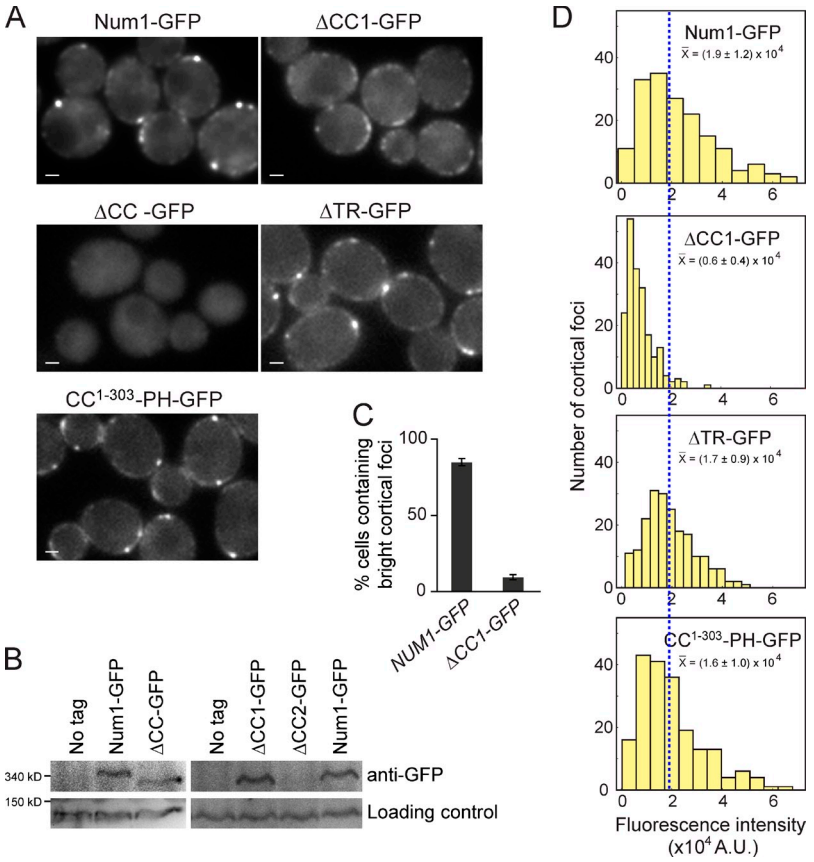

Figure 2. **N-terminal predicted coiled-coil region of Num1 is required for cortical patch assembly.** (A) Wide-field single–focal plane images of live cells expressing chromosomally tagged GFP fusion of Num1 constructs. Bars, 1 µm. (B) Western blots of indicated Num1 constructs tagged with GFP. (C) Loss of bright cortical foci in *ΔCC1-GFP* cells. *NUM1-GFP mCherry-TUB1* and *ΔCC1-GFP* cells, distinguished by mCherry-Tub1 labeling, were imaged in the same field. The percentage of cells exhibiting cortical GFP foci with an intensity >7,700 (arbitrary units) was plotted (n > 228 cells for each strain). Error bars are standard error of proportion. (D) Histograms of fluorescence intensity for individual cortical foci of Num1-GFP, ΔCC1-GFP, ΔTR-GFP, and $CC^{1–303}$-PH-GFP ($n \geq$ 173 foci for each construct from a single experiment). $\bar{x}$ denotes mean ± SD. The blue dashed line indicates the mean intensity of Num1-GFP foci. A.U., arbitrary unit.

only the coiled-coil region and the PH domain by deleting aa 304–2,562. Strikingly, this construct, hereafter termed $CC^{1–303}$-PH (Fig. 1), assembled cortical patches indistinguishable from the full-length Num1 patches (Fig. 2, A and D). Another truncation mutant, termed ΔTR, which retained the EF-hand but was otherwise identical to $CC^{1–303}$-PH, also formed normal patches (Figs. 1 and 2 [A and D]). Additionally, deletion of the N-terminal aa 2–103, but not aa 2–94, abolished bright patch assembly (Fig. S1 D). These results suggest that the sequence required for patch assembly extends from residues 95 to 303.

Num1 mutants defective in patch assembly failed to anchor dynein

Next, we performed a cold nuclear segregation assay to evaluate the function of our Num1 constructs in the dynein pathway. *ΔCC-GFP* and *ΔCC1-GFP* strains, both defective in patch formation (Fig. 2 A), had 16.9 and 15.4% binucleated cells, respectively, similar to what was observed for *num1Δ* (19.3%; Fig. 3 A), indicating defective dynein pathway function in these cells (Geiser et al., 1997; Heil-Chapdelaine et al., 2000). Strikingly, the *$CC^{1–303}$-PH* strain had only 0.6% binucleated cells (Fig. 3 A), indicating that deleting aa 304–2,562 did not interfere with nuclear segregation. *ΔEF* and *ΔTR* strains had <1% binucleated cells (Figs. 3 A and S1 B), consistent with *$CC^{1–303}$-PH*. Furthermore, deleting the first 94 aa did not affect Num1 function (*ΔN* strain, <1% binucleated cells), whereas deleting the last 65 aa partially disrupted Num1 function (*ΔC* strain, 6.7% binucleated cells; Fig. S1 B). Collectively, these results show that aa 1–303 (encompassing the CC1 and CC2 motifs) and aa 2,563–2,748 (encompassing the PH and C domains) are two regions of Num1 required for its function in the dynein pathway. Similar results were obtained by assaying for spindle misorientation using GFP-labeled tubulin (Fig. S2 D).

Next, we examined *num1* mutants for synthetic growth defects with *kar9Δ*. Budding yeast need either the dynein or Kar9 pathway for normal growth (Miller et al., 1999; Yin et al., 2000; Lee et al., 2005). Tetrad dissection analysis showed that *num1Δ kar9Δ* double mutants grew poorly, forming microcolonies (Table 1). Consistent with the binucleate data, *kar9Δ* mutant showed synthetic growth defects with *ΔCC1* and *ΔCC* but not with *$CC^{1–303}$-PH* and *ΔTR* (Table 1).

To measure dynein anchoring in the *num1* mutants more directly, we assayed for cortical localization of dynein heavy chain (HC) Dyn1/HC. We examined time-lapse two-color images of Dyn1-3GFP and mCherry-Tub1, scoring for cortical foci that were stationary and free from association with astral microtubules. We observed cortical Dyn1-3GFP foci in *$CC^{1–303}$-PH* and *ΔTR* strains but not in *ΔCC1* and *ΔCC* strains (Figs. 3 C and S2 A). In *$CC^{1–303}$-PH* and *ΔTR* cells, the frequency of finding cortical Dyn1-3GFP foci was reduced (Fig. 3 B), but the intensity of individual foci was not significantly different from that in wild type (Fig. 3 D), indicating a defect in dynein targeting efficiency. We also observed cortical dynactin Jnm1-3mCherry foci in *$CC^{1–303}$-PH* cells (Fig. S2 C), and, as reported for wild-type cells (Moore et al., 2008), this targeting depended on Dyn1/HC (Fig. S2 C, bottom row).

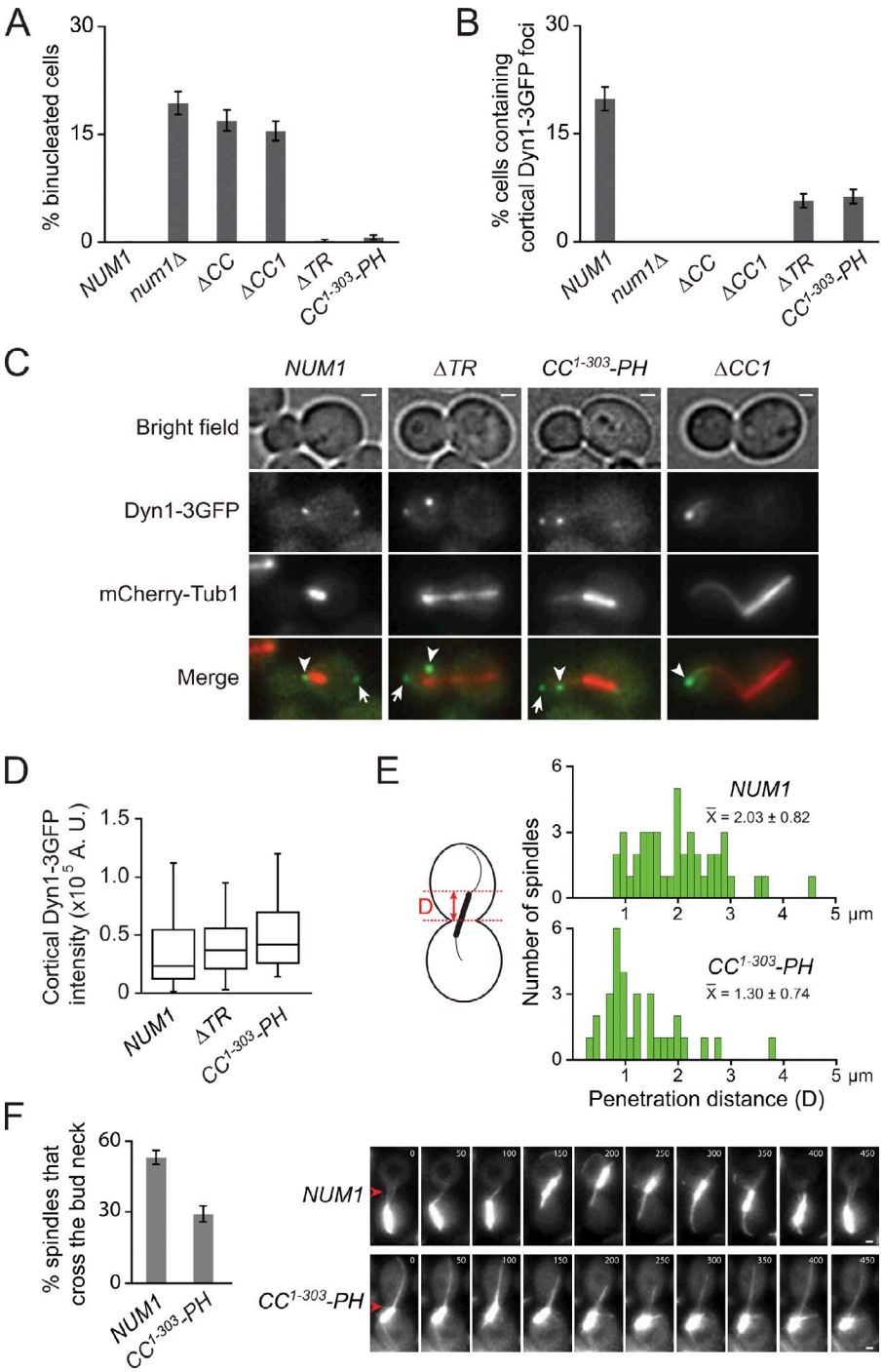

Figure 3. **$CC^{1–303}$-PH is defective for spindle oscillations but is otherwise sufficient for dynein-dependent spindle positioning.** (A) The percentage of binucleated cells in cultures grown at 12°C for 16 h ($n \geq 495$ cells for each strain). (B) The percentage of cells exhibiting stationary cortical Dyn1-3GFP foci ($n \geq 539$ cells for each strain). (C) Cells expressing Dyn1-3GFP and mCherry-Tub1. Arrows indicate stationary cortical Dyn1-3GFP foci, and arrowheads indicate motile plus-end Dyn1-3GFP foci, as determined by two-color videos. Bars, 1 µm. (D) Box plot of cortical Dyn1-3GFP intensity. Foci in *ΔTR* and *$CC^{1–303}$-PH* strains were not significantly different from those in wild-type *NUM1* ($P > 0.02$ by a *t* test; $n \geq 20$ foci for each strain). A.U., arbitrary unit. (E) Histograms of spindle penetration distance in HU-arrested *NUM1* or *$CC^{1–303}$-PH* cells in the *kar9Δ* background. Distance of spindle penetration, denoted by a red D, is defined as the farthest distance traveled by a spindle pole moving across the bud neck during a 10-min video ($P = 0.0002$ for *$CC^{1–303}$-PH* vs. *NUM1* by a *t* test; $n \geq 32$ spindles for each strain from a single experiment). $\bar{x}$ denotes mean ± SD. (F, left) The percentage of spindles in HU-arrested *NUM1 kar9Δ* or *$CC^{1–303}$-PH kar9Δ* cells that crossed the bud neck over the course of a 10-min video ($P < 0.0001$ by a *t* test; $n \geq 181$ for each strain from a single experiment). (right) Examples of GFP-Tub1 time-lapse images used for quantification. Time is in seconds. Arrowheads mark the bud neck. Bars, 1 µm. All error bars are standard error of proportion.

To detect possible functional defects for *$CC^{1–303}$-PH*, we performed a spindle oscillation assay, scoring for spindle movement through the bud neck in hydroxyurea (HU)-arrested cells in a *kar9Δ* background. This assay assesses dynein-mediated spindle movement in the absence of spindle elongation (Moore et al., 2009a; Stuchell-Brereton et al., 2011). Compared with *NUM1*, the *$CC^{1–303}$-PH* mutant exhibited a significantly lower frequency of finding a spindle moving across the bud neck (Fig. 3 F, left). Moreover, in cells where the spindle was able to enter the bud neck, it moved for a significantly shorter distance (Fig. 3 E). However, the velocity of spindle movement was similar in *NUM1* and *$CC^{1–303}$-PH* cells (Fig. S2 B). These analyses revealed a compromised dynein activity in the *$CC^{1–303}$-PH* strain, albeit without resulting in a nuclear segregation phenotype.

Mapping Num1 interaction with the dynein complex

As the *$CC^{1–303}$-PH* strain exhibited dynein pathway function, we reasoned that $CC^{1–303}$ might possess a binding site for the recruitment of dynein, either directly or indirectly, to the cell cortex. We biochemically isolated recombinant GST fragments of Num1 from bacteria and used them to assay for pull-down of dynein from yeast cell lysates. We found that

Table 1. **Viability of *num1* alleles in combination with *kar9Δ* mutant**

Mutant crossed with *kar9Δ*	No. of tetrads analyzed	No. of predicted double mutants	Viability of double mutant	
			Microcolony	Viable
num1Δ	11	12	12	–
NUM1-GFP	12	12	–	12
ΔCC-GFP	14	14	14	–
ΔCC1-GFP	14	10	10	–
ΔTR-GFP	13	12	–	12
$CC^{1–303}$*-PH-GFP*	16	20	–	20
$CC^{1–303}$*-GFP*	12	13	13	–
$CC^{1–303}$*-GFP-CAAX*	21	23	–	23
$num1^{L167E + L170E}$	12	13	13	–

Indicated strains were crossed with *kar9Δ*. The resulting diploid strains were sporulated, and tetrads were dissected.

GST-$CC^{1–303}$ was insoluble, but a slightly larger construct, GST-$CC^{1–325}$, was soluble. Fig. 4 A (left) shows that affinity-purified GST-$CC^{1–325}$, but not the GST control, pulled down Pac11/intermediate chain from a yeast extract expressing endogenously tagged Pac11-13Myc. GST-$CC^{1–325}$ also pulled down $Dyn1_{TAIL}$-3GFP (Fig. 4 A, left), an N-terminal tail fragment of Dyn1/HC that has been shown to colocalize with full-length Num1 at the cell cortex (Markus et al., 2009). Additionally, another soluble recombinant construct, $CC^{95–303}$ fused to an S tag, specifically pulled down Pac11-13Myc and $Dyn1_{TAIL}$-3GFP from the respective cell lysates (Fig. 4 A, right). The observed pull-downs were abolished when Nip100, the $p150^{Glued}$ subunit of dynactin, was removed from the cell lysates (Fig. 4 A, right), indicating that the interaction between $CC^{95–303}$ and dynein depends on dynactin.

Next, we tested for in vivo association of $CC^{1–303}$ with Dyn1/HC using the bimolecular fluorescence complementation (BiFC) assay (Shyu et al., 2008). Dyn1 and $CC^{1–303}$ (or full-length Num1) were respectively fused to the N- and C-terminal half of Venus (VN and VC, respectively) and expressed under the control of the endogenous promoter. Cells expressing both Dyn1-VN and VC-Num1 exhibited cortical fluorescent Venus foci that were reminiscent of cortical Num1 patches (Fig. 4 B, top rows). These foci were not detected in cells expressing only Dyn1-VN, VC-Num1, or VC-$CC^{1–303}$ (Fig. S3 A), indicating that they were specific signals as a result of the interaction between Dyn1/HC and Num1. In cells expressing Dyn1-VN and VC-$CC^{1–303}$, we observed Venus foci at the spindle pole bodies (SPBs; Fig. 4 B, bottom row), indicating an in vivo association of $CC^{1–303}$ with Dyn1/HC. We did not observe Venus foci at the cortex of these cells, presumably because $CC^{1–303}$ failed to localize there (Fig. 5 B) and also because Dyn1/HC was absent from the cortex as a result of the lack of a functional Num1 (VC-$CC^{1–303}$ was the only source of Num1 in these cells). We also did not observe Venus foci at the plus end of astral microtubules, suggesting that there might be a regulatory mechanism preventing Dyn1/HC from binding to Num1 at the plus end without being anchored at the cell cortex. Consistent with this notion, we found that overexpressed GFP-tagged $CC^{1–325}$ was absent from the plus end (Fig. S3 B).

Next, we asked whether overexpression of $CC^{1–325}$ would inhibit dynein function, as would be expected if $CC^{1–325}$ competes with full-length Num1 for interaction with Pac11/intermediate chain and Dyn1/HC. When $CC^{1–325}$ was coexpressed with wild-type Num1 in a diploid strain using the endogenous *NUM1* promoter, it had no effect on the dynein pathway function, resulting in <0.5% of binucleated cells ($CC^{1–325}$*/NUM1*; Fig. 4 C, left). However, when the expression of $CC^{1–325}$ was induced by the *GAL1* promoter (Fig. 4 C, right), the frequency of binucleated cells increased to 14.0% (*GAL1p-*$CC^{1–325}$*/NUM1*; Fig. 4 C, left), demonstrating that overexpression of $CC^{1–325}$ interferes with dynein pathway function. Collectively, our results demonstrate that the N-terminal region of Num1 encompassing the CC1 and CC2 motifs interacts with dynein in a dynactin-dependent manner and that this interaction is required for dynein-mediated nuclear segregation.

The PH domain is dispensable for Num1 patch assembly and function

To further test the idea that the PH domain is required solely for the initial recruitment of Num1 to the membrane, we asked whether $CC^{1–303}$ would assemble patches if targeted to the cell cortex via a different mechanism. We found that $CC^{1–303}$-GFP was diffuse in the cytoplasm (Fig. 5 B) but assembled cortical patches when fused to a CAAX motif (GSGGCCIIS from Ras2; Deschenes and Broach, 1987; Finegold et al., 1990; Srinivasa et al., 1998). $CC^{1–303}$-GFP-CAAX patches were strikingly similar to those observed for Num1-GFP and $CC^{1–303}$-PH-GFP (Figs. 2 A and 5 B). In contrast, GFP-CAAX did not form cortical patches but exhibited weak fluorescent signals along the cell membrane (Fig. 5 B), suggesting that $CC^{1–303}$ indeed directs bright patch formation at the cell cortex.

Next, we asked whether $CC^{1–303}$-GFP-CAAX patches could rescue the dynein pathway function. In a cold nuclear segregation assay, the $CC^{1–303}$*-GFP-CAAX* strain exhibited 2.6% binucleated cells, whereas a *num1Δ* mutant exhibited 16.2% (Fig. 5 C). In common with wild-type and $CC^{1–303}$*-PH* cells, cortical dynactin Jnm1-3mCherry foci were observed in $CC^{1–303}$*-GFP-CAAX* cells (Fig. S2 C). Furthermore, tetrad analysis showed that all $CC^{1–303}$*-GFP-CAAX kar9Δ* double mutants grew normally, whereas $CC^{1–303}$*-GFP kar9Δ* double

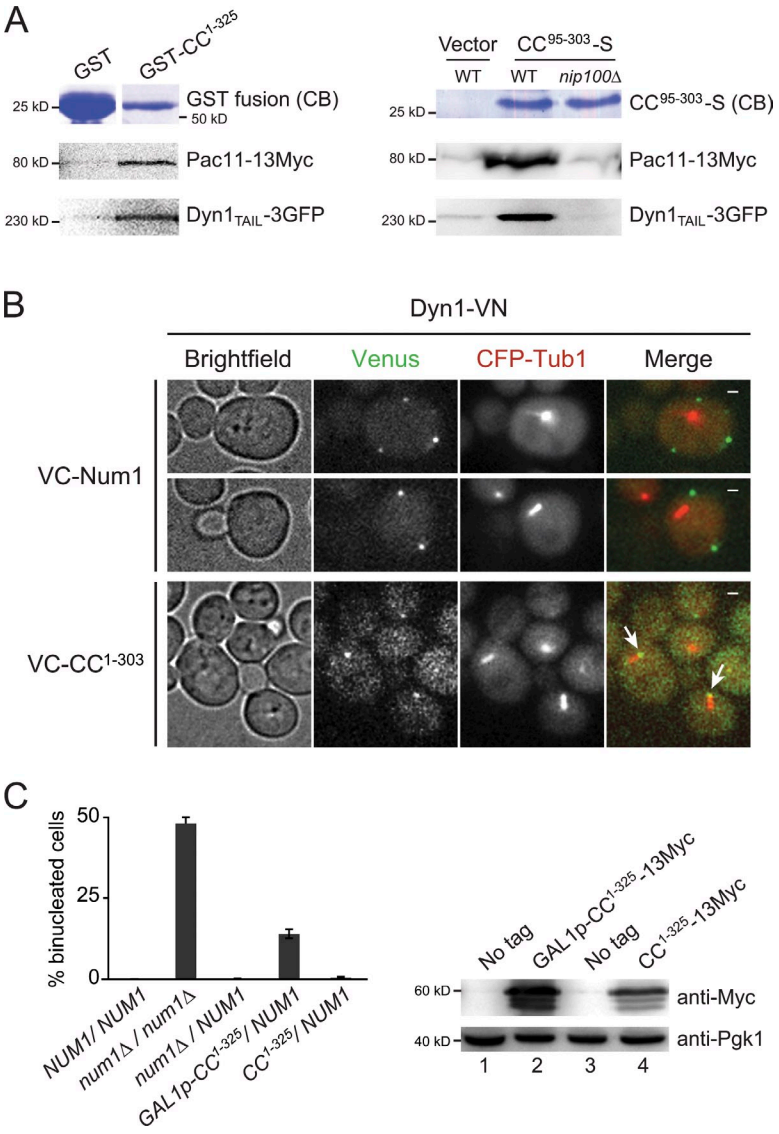

Figure 4. **CC fragments interact with the dynein complex.** (A) Dynein pull-down assays. Yeast extracts expressing Pac11-13Myc or $Dyn1_{TAIL}$-3GFP were incubated with GST fusion proteins (top left) or S-tagged proteins (top right) immobilized on glutathione beads or S-protein agarose, respectively. Bound proteins were eluted and analyzed by immunoblotting (middle and bottom). CB, Coomassie blue; WT, wild type. (B) In vivo interaction of $CC^{1–303}$ with Dyn1 in the BiFC assay. The N- and C-terminal fragment of Venus, VN and VC, respectively, were fused to the C terminus of Dyn1 and the N terminus of Num1 or $CC^{1–303}$. Fluorescence as a result of reconstitution of the Venus fluorophore was acquired in the YFP channel. Arrows indicate Venus foci at the SPB. Bars, 1 µm. (C, left) The percentage of binucleated cells in cultures grown in YP media containing 2% raffinose and 2% galactose at 12°C for 16 h. Error bars are standard error of proportion ($n > 600$ cells for each strain). (right) A Western blot of total cell lysates prepared from cultures indicated on the left. Pgk1 was used as a loading control. The $CC^{1–325}$-13Myc level induced by the *GAL1* promoter (lane 2) was 2.4-fold higher than that expressed by the endogenous *NUM1* promoter (lane 4).

mutants formed microcolonies (Table 1). These results demonstrate that CAAX-targeted $CC^{1–303}$-GFP rescues the dynein pathway function in the absence of a full-length Num1.

Mapping Num1 domain for cortical mitochondrial attachment

Num1 has been implicated in mitochondrial attachment and division through an Mdm36-dependent interaction with Dnm1 at the cell cortex (Cerveny et al., 2007; Hammermeister et al., 2010). Thus, we quantified mitochondrial attachment in our *num1* mutants, using Cox4-RFP to label the mitochondria and calcofluor to mark the cell periphery. Mitochondria were attached to the cell cortex in *$CC^{1–303}$-PH* and *$CC^{1–303}$-GFP-CAAX* cells (Fig. 5, D [arrowheads] and E). However, in the *ΔCC1* mutant, mitochondria were mostly dissociated from the cell cortex, primarily seen clustered in the cell center, as in the *num1Δ* mutant (Fig. 5, D and E). Time-lapse videos of Cox4-RFP showed that mitochondrial tubules were attached to the cell cortex at various points in wild type, *$CC^{1–303}$-PH*, and *$CC^{1–303}$-GFP-CAAX* (Videos 1, 4, and 5). Mitochondria fission events were also detected in these cells (arrowheads in videos), indicating functional mitochondrial division machinery. In contrast, in *ΔCC1* (Video 3), mitochondria often appeared as interconnected nets of tightly packed tubules detached from the cell cortex, strikingly similar to that observed in *num1Δ* (Video 2). The frequency with which mitochondria were observed attached to the cell cortex in a video of *$CC^{1–303}$-PH* or *$CC^{1–303}$-GFP-CAAX* was indistinguishable from that of wild type, indicating that the N-terminal 1–303 aa of Num1 is sufficient for cortical mitochondrial attachment function. Furthermore, consistent with a role that is independent of the dynein pathway function (Cerveny et al., 2007; Hammermeister et al., 2010), cortical mitochondrial attachment in *$CC^{1–303}$-PH* and *$CC^{1–303}$-GFP-CAAX* cells was unaffected when Dyn1/HC or Nip100 was deleted (Fig. 5 E and Video 6).

Self-association of Num1 mediated by the $CC^{95–303}$ domain

We sought to understand the mechanism of patch assembly mediated by the coiled-coil region, which is highly conserved

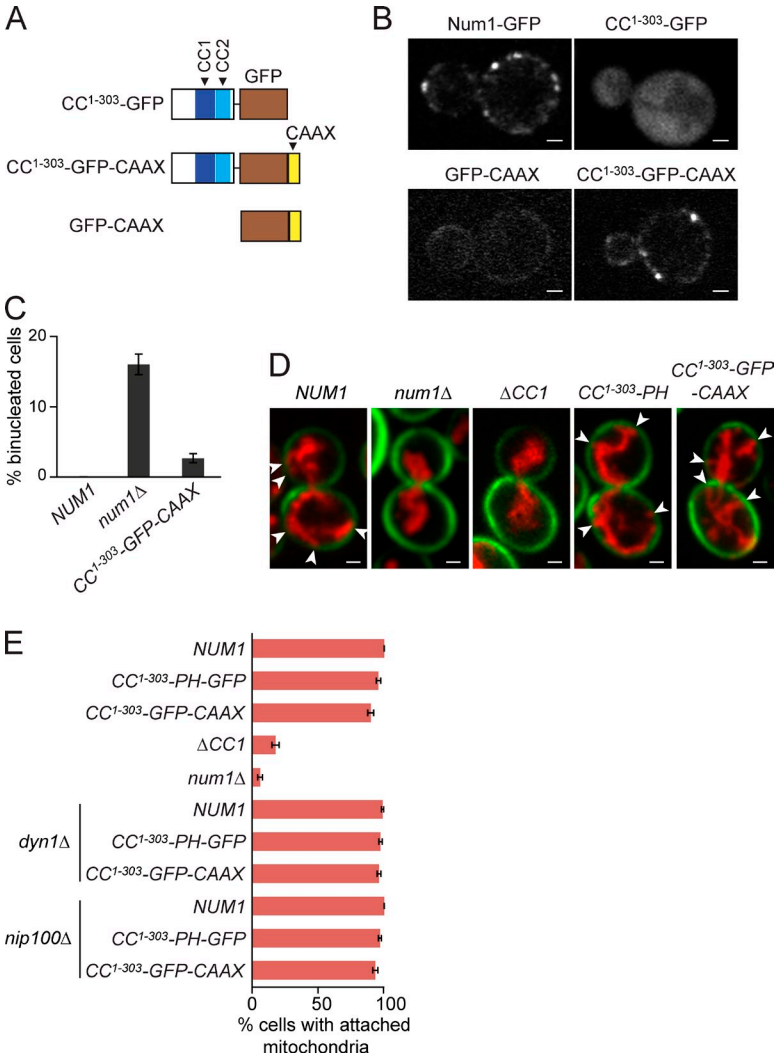

Figure 5. **Num1 PH domain is dispensable for cortical patch assembly.** (A) Diagram of $CC^{1–303}$ fusion with GFP or GFP-CAAX. (B) Confocal images of live cells expressing chromosomally tagged GFP constructs expressed by the *NUM1* promoter. Bars, 1 µm. (C) The percentage of binucleated cells in cultures grown at 12°C for 16 h ($n > 600$ cells for each strain). (D) Cortical attachment of mitochondria. Cells expressing Cox4-RFP (red) were fixed and stained for cell periphery with calcofluor (green). Each image is a maximum intensity projection of a 0.8-µm z stack of confocal images. Arrowheads indicate visible association of mitochondria with the cell cortex. Bars, 1 µm. (E) The percentage of cells in which mitochondria were attached to the cell cortex. Cortical attachment of mitochondria was determined from videos of calcofluor-stained cells expressing Cox4-RFP ($n \geq 156$ cells for each strain). All error bars are standard error of proportion.

among Num1 homologs in various fungal species (Fig. S1 C), including the evolutionarily distant *Schizosaccharomyces pombe* (Saito et al., 2006; Yamashita and Yamamoto, 2006). As BLAST (basic local alignment search tool) searches using aa 1–340 of Num1 did not reveal any significant sequence similarities to protein domains of known function, we sought to identify higher-order structural homologs using the I-TASSER (iterative threading assembly refinement) program (Roy et al., 2010). Strikingly, all top 10 domain hits predicted to be structurally similar to the Num1 coiled-coil region are either F- or N-Bin/Amphiphysin/Rvs (BAR) domains from proteins such as FCHo2, syndapin/PACSIN, endophilin-III, ARFAPTIN, and Bin1/Amphiphysin II. Fig. S4 shows the predicted structure of $CC^{1–340}$ and its similarity with the FCHo2 F-BAR domain. BARs are known protein modules that can both sense and bind membrane curvature, with an important biochemical propensity to form homodimers (Peter et al., 2004; Itoh et al., 2005; Henne et al., 2007; Shimada et al., 2007; Frost et al., 2008; Wang et al., 2009). We tested whether $CC^{1–325}$ would interact with itself by carrying out a coimmunoprecipitation experiment. $CC^{1–325}$-13Myc specifically coprecipitated with $CC^{1–325}$-3HA and vice versa (Fig. 6 A). Furthermore, analytical gel filtrations of purified $CC^{95–303}$ (a soluble construct) showed that it migrated as a single peak corresponding to a 232-kD globular protein (Fig. 6, B and C), markedly larger than the molecular mass calculated from its amino acid composition (28.6 kD). The elution in low (150 mM NaCl) or high (500 mM NaCl) salt gave similar results, yielding a Stokes radius of 5.07 nm. Interestingly, further analysis of the peak gel-filtered fractions by sedimentation equilibrium (Fig. 6 D) revealed that the molecular mass of the $CC^{95–303}$ species was 58.2 kD, consistent with a homodimer of $CC^{95–303}$. Together, these biochemical results indicate that $CC^{95–303}$ dimerizes in solution to form a molecule with an elongated shape, a characteristic shared by all known BAR domains (Shimada et al., 2007; Frost et al., 2008; Wang et al., 2009).

Targeted mutations in the Num1 BAR-like domain differentially disrupt patch assembly and dynein function

BAR domains form crescent-shaped antiparallel dimers that can further polymerize tip to tip into filaments for membrane association and tubulation (Shimada et al., 2007; Frost et al., 2008; Karotki et al., 2011). We hypothesized that a similar tip-to-tip interaction mediates aggregation of $CC^{95–303}$ dimers into morphologically distinct patches. A point mutation located at the tip (see Fig. S4 A) of the crescent-shaped F-BAR dimer has

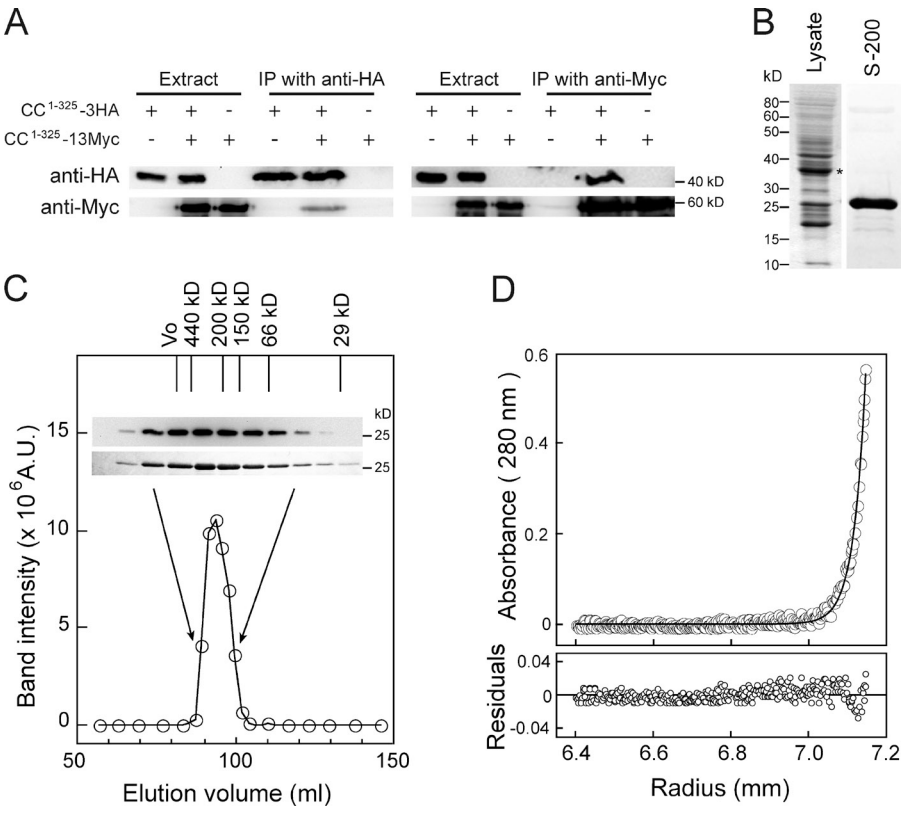

Figure 6. **PA domain is an elongated homodimer.** (A) $CC^{1–325}$-3HA coimmunoprecipitated with $CC^{1–325}$-13Myc and vice versa. Total extracts from diploid strains expressing *GAL1p*-induced $CC^{1–325}$-13Myc or $CC^{1–325}$-3HA or both were immunoprecipitated (IP) with anti-HA (left) or anti-Myc antibody (right). Bound proteins were probed as indicated. (B) Purification of $CC^{95–303}$. Lysate denotes bacterial extract expressing $CC^{95–303}$-S-TEV-Z (indicated by an asterisk), and S-200 indicates pooled fractions of $CC^{95–303}$-S after TEV digestion and Sephacryl S-200 gel filtration chromatography. (C) Analytical gel filtration of $CC^{95–303}$-S. Elution of $CC^{95–303}$-S from a calibrated Sephacryl S-200 column was analyzed by Western blotting with an anti–S tag antibody (top blot) or by Coomassie staining (bottom blot). $CC^{95–303}$-S migrates as a single peak with an apparent molecular mass of 232 kD and a Stokes radius of 5.07 nm. A.U., arbitrary unit. (D) Sedimentation equilibrium of S-200–purified $CC^{95–303}$-S at 28,000 rpm. The distribution of $CC^{95–303}$-S at equilibrium was fitted using the nonlinear least square method of HeteroAnalysis (Cole, 2004). Mass = 58,184 D. Residuals from fitting are shown at the bottom.

been shown to abolish the tip-to-tip interaction between F-BAR dimers (Shimada et al., 2007; Frost et al., 2008). Using our predicted $CC^{1–340}$ structure (Fig. S4 B), we identified two residues located at the analogous tip, E191 and K192, and mutated both to alanine in the full-length Num1 protein (Fig. 1). Analytical gel filtration confirmed that the E191A + K192A mutation (hereafter referred to as EK mutation) did not affect the dimerization of $CC^{95–303}$ (Fig. S3 C). In support of our hypothesis, we found that GFP-tagged $Num1^{EK}$ was defective in bright patch assembly when compared with wild-type Num1 (Fig. 7 A). The percentage of cells exhibiting bright foci (Fig. 7 B) as well as the total number of observed bright foci (Fig. 7 C, blue dashed line)—i.e., those with intensity higher than the mean intensity of wild-type Num1-GFP—were significantly reduced in the *num1^{EK}-GFP* strain. Interestingly, the targeted EK mutation only caused 1% of binucleated cells (Fig. 7 D), indicating the existence of cortical dynein activity. However, in a spindle oscillation assay, the EK mutation decreased the frequency of observing spindle movement into the bud neck by 55% (Fig. 7 E, left). Of the spindles that moved into the neck, the penetration distance was significantly shorter than that in wild-type cells (1.6 ± 0.7 vs. 2.2 ± 0.9 µm; P = 0.0011; Fig. 7 E, right), indicating a partially impaired cortical dynein activity. Additionally, *num1^{EK}* cells exhibited Dyn1-3GFP foci at the cell cortex (Fig. S3 D) but at a frequency 3.3-fold lower than that observed in wild-type cells (Fig. 8 A). These results, along with the biochemical characterizations of $CC^{95–303}$ (Fig. 6), provide strong evidence for a BAR-like domain in mediating the assembly of Num1 patches.

As the BAR-like domain is also involved in mediating dynein interaction (Fig. 4, A and B), we wondered whether the dynein-anchoring function could be specifically disrupted without affecting patch assembly. We screened for the dynein-binding site by site-directed mutagenesis, choosing candidate residues using the predicted $CC^{1–340}$ structure. Residues along the helices of the wing structure were targeted (see Fig. S4 B), whereas residues within the putative dimerization region were avoided, as the latter is likely important for the formation of the crescent-shaped structure and hence tip-to-tip mediated patch assembly. We found that L167 and L170, two residues located within the CC1 motif, are specifically required for the dynein-anchoring function of Num1. Cells expressing $Num1^{L167E + L170E}$ (both residues mutated to Glu; hereafter referred to as $Num1^{LL}$) exhibited cortical patches indistinguishable from wild-type Num1 (Fig. 8 B) but behaved like *num1Δ* in the cold nuclear segregation assay, accumulating 19.6% of binucleated cells (compared with 21.4% for *num1Δ*; Fig. 7 D). Other residues that we had targeted, as shown in Fig. S4 B, neither resulted in a binucleate nor a patch assembly phenotype. Consistent with the high binucleate level, we failed to detect cortical Dyn1/HC foci and Jnm1/dynamitin foci in *num1^{LL}* cells (Fig. 8 C). Rather, these cells exhibited an enhancement of Dyn1-3GFP and Jnm1-3mCherry levels at the plus end of astral microtubules (Fig. 8 C), another phenotype similar to *num1Δ* (Lee et al., 2003; Sheeman et al., 2003). Additionally, *num1^{LL}* showed synthetic growth defect with *kar9Δ* (Table 1). However, we found that the mitochondria in *num1^{LL}* cells were morphologically similar to those in wild-type cells, displaying no apparent defect in their attachment to the cell cortex (Video 7). We conclude that the L167E + L170E mutation specifically abolished the dynein-anchoring activity of Num1, uncoupling it from patch assembly and mitochondrial attachment functions.

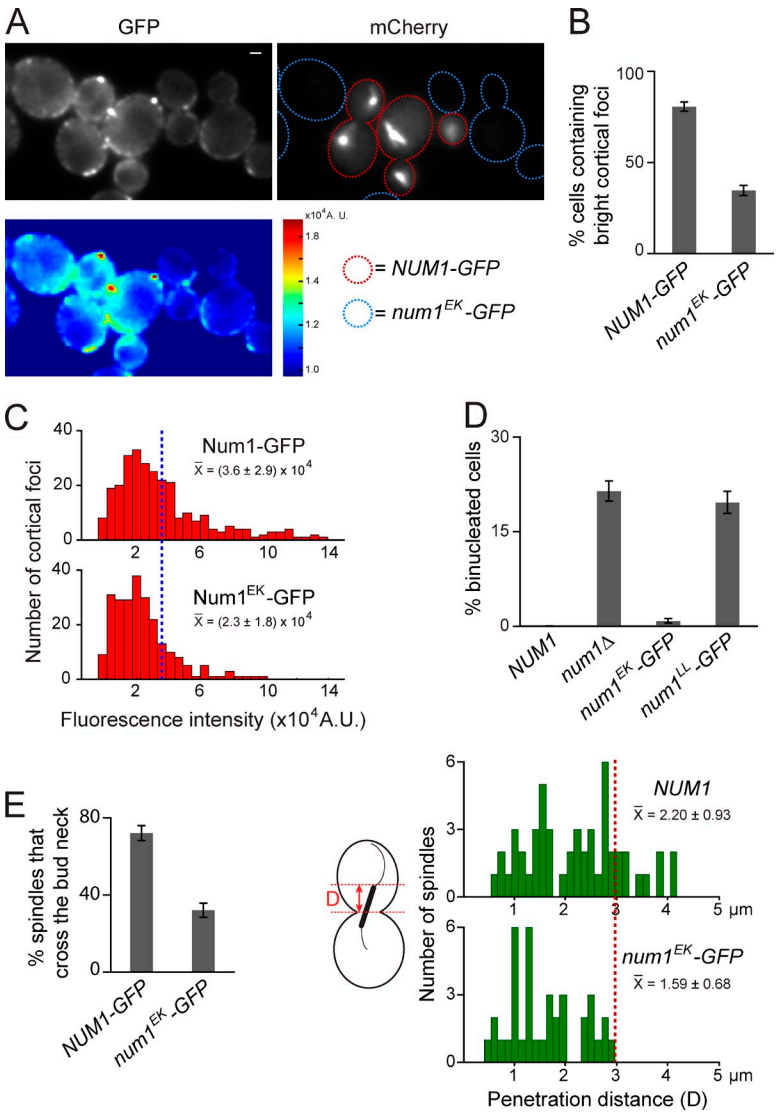

Figure 7. **E191A + K192A (EK) mutation in Num1 disrupts patch assembly function.** (A) *NUM1-GFP mCherry-TUB1* cells were imaged in the same field with *num1^{EK}-GFP* cells. (top) Single–focal plane image of GFP and mCherry-Tub1. (bottom) A color intensity map showing that *NUM1-GFP* cells, but not *num1^{EK}-GFP*, exhibit bright cortical GFP patches. A.U., arbitrary unit. Bar, 1 µm. (B) The percentage of cells in A exhibiting cortical GFP foci with intensities >18,000 (arbitrary units; $n \geq 237$ cells for each strain). (C) Histograms of fluorescence intensity of individual Num1-GFP or Num1^{EK}-GFP cortical foci ($n \geq 239$ foci for each construct from a single experiment). $\bar{x}$ denotes mean ± SD. The blue dashed line indicates the mean intensity of Num1-GFP foci. The mean value of Num1-GFP is different from that in Fig. 2 D because of nonidentical imaging conditions. (D) The percentage of binucleated cells in cultures grown at 12°C for 15 h ($n \geq 510$ cells for each strain). (E) *num1^{EK}* cells exhibited defects in moving the spindle. (left) The percentage of spindles that crossed the bud neck during a 10-min video for HU-arrested *NUM1* and *num1^{EK}* cells in the *kar9Δ* background ($P < 0.0001$ by *t* test; $n \geq 133$ spindles for each strain from a single experiment). (right) Histograms of penetration distance (as defined in Fig. 3 E) during spindle oscillation. $P = 0.001$ by a *t* test ($n \geq 37$ spindles for each strain from a single experiment). $\bar{x}$ denotes mean ± SD. The red dashed line indicates that spindles in *num1^{EK}* cells failed to move for a distance >2.9 µm. All error bars are standard error of proportion.

Discussion

Anchorage at the cell cortex is crucial for dynein to exert pulling forces on astral microtubules to position the mitotic spindle in a dividing cell. Here, we have identified a domain in Num1 that is specifically required for mediating dynein interaction at the cell cortex. Another function of this domain is to mediate the assembly of characteristic Num1 patches at the cell cortex. Because of this latter function, we propose to name this domain PA domain (aa 1–303).

We were surprised to find that, in addition to its function in the dynein pathway, the PA domain is also sufficient for mediating cortical mitochondrial attachment. Interestingly, an L167E + L170E mutation in the PA domain completely abolished cortical dynein localization (Fig. 8, A and C) but did not affect mitochondrial morphology or mitochondrial attachment at the cortex (Video 7). Also, in common with previously reported unpublished data (Cerveny et al., 2007), we found that dynein and dynactin are not required for mitochondria shape and distribution (Fig. 5 E and Video 6). These observations suggest that although the PA domain mediates both dynein anchoring and mitochondrial attachment at the cortex, the underlying mechanisms regulating these processes might be different.

The PA domain is located in the predicted coiled-coil region of Num1. Deletion of the first or both of the coiled-coil motifs resulted in defects in cortical patch formation and a spindle mispositioning phenotype. In agreement with our results, a previous study reported that a Num1 truncation mutant lacking the entire N-terminal half of the protein (thus lacking the PA domain) failed to complement the dynein pathway function (Farkasovsky and Küntzel, 1995). The truncated Num1 mutant, expressed from a plasmid as a fusion protein to the Gal4 DNA–binding domain, showed no difference in localization compared with wild-type Num1 by indirect immunofluorescence microscopy, a result that appears to be in contrast to our data. This observed discrepancy may be partly explained by differences in the approaches used for the respective localization studies. It may also reflect a difference between episomal versus chromosomal expression or, alternatively, a result of the fusion to the Gal4 DNA–binding domain.

Our results demonstrate that the PA domain functions as the minimal dynein-binding domain, as it was sufficient for rescuing

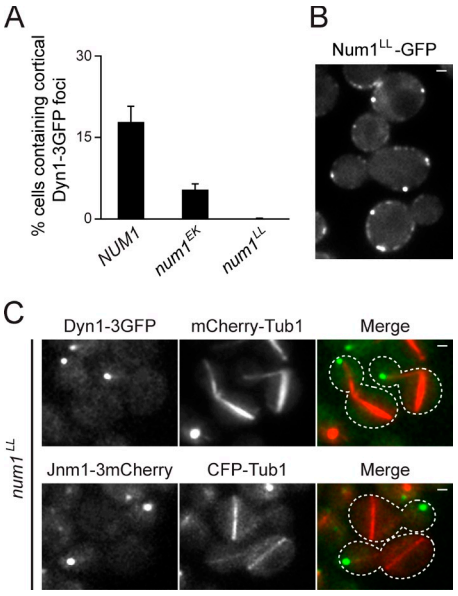

Figure 8. **L167E + L170E (LL) mutation in Num1 specifically disrupts dynein-anchoring but not patch assembly function.** (A) The percentage of cells exhibiting stationary cortical Dyn1-3GFP foci. Error bars are standard error of proportion (n = 179 for *NUM1*, 500 for *num1*^{LL}, and 539 for *num1*^{EK}). (B) Single–focal plane image of live cells expressing chromosomally tagged Num1^{LL}-GFP. (C) *num1*^{LL} cells expressing Dyn1-3GFP and mCherry-Tub1 or Jnm1-3mCherry and CFP-Tub1 showing loss of cortical dynein and dynactin foci. Each image is a maximum intensity projection of a 2-µm z stack of widefield images. Dotted lines outline the cell. Bars, 1 µm.

nuclear segregation when fused to either a PH domain or a CAAX motif. Additionally, isolated fragments of the PA domain have the ability to associate with dynein (Fig. 4, A and B). During the asymmetric cell division in mammals, it is thought that astral microtubule plus-end–associated dynein achieves cortical association through binding to cortical nuclear mitotic apparatus protein (NuMA; Du and Macara, 2004; Poulson and Lechler, 2010; Williams et al., 2011). NuMA in turn binds to LGN (Bowman et al., 2006; Izumi et al., 2006; Siller et al., 2006), which is recruited to the cell cortex via its C-terminal GoLoco motifs by binding to the glycosylphosphatidylinositol-linked G-α_i/G-α_o (Du and Macara, 2004; Blumer et al., 2006; Johnston et al., 2009; Ségalen et al., 2010; Woodard et al., 2010). Therefore, cortical association and membrane tethering functions of the dynein–dynactin complex in mammals appear to be performed by different proteins rather than by two different domains within the same protein, as we have described here for Num1.

Our data suggest that the assembly of morphologically distinct Num1 patches does not appear to be a prerequisite for dynein anchoring. This idea is supported by the observation of cortical dynein foci in *num1*^{EK} cells that are defective in bright patch formation (Fig. S3 D). However, *num1*^{EK} cells exhibited significant defects in spindle movement that are indicative of compromised dynein activity (Fig. 7 E), arguing that the pulling force generated by dynein might be reduced in this mutant. The force reduction could be caused either by a reduction in the frequency of cortical dynein targeting (Fig. 8 A) or a weaker cortical anchoring of dynein to the membrane by the Num1^{EK} construct as a result of defective patch assembly. Thus, patch formation of Num1 may enhance the cortical anchoring of dynein, presumably by strengthening the connection between dynein and Num1 and/or the association between Num1 and the cell membrane. Given the very mild binucleate phenotype observed in the *num1*^{EK} mutant, it is possible that the patch formation–mediated enhancement of dynein activity is required only at a specific time or under a specific context during the cell division cycle, i.e., situations where a high force production by dynein is necessary, such as during the initial movement of the nucleus into the narrow bud neck (Moore et al., 2009a). One may argue that the lack of a severe phenotype in nuclear segregation might be attributable to incomplete disruption of bright patch formation. However, we noticed attenuated spindle movement in *CC*$^{1–303}$*-PH* cells, which exhibited normal patch assembly (Fig. 3, E and F), thus suggesting that the observed phenotype in *num1*^{EK} cells could be explained by a lower degree of dynein motor force.

Unlike the distribution of PI(4,5)P_2, which appears fairly homogeneous at the cell membrane as determined by $PH_{PLC\delta1}$-GFP labeling (Mendoza et al., 2009), Num1 patches adopt a punctate pattern at the cell cortex, indicating that the PA domain must recognize a cortical landmark that specifies sites for patch assembly. What is the landmark? One hypothesis is that it is a plasma membrane–bound protein to which the PA domain binds specifically. This membrane protein may function like a scaffold, having multiple binding sites to allow docking of multiple Num1 molecules, facilitating the formation of a Num1 patch. However, as the PA domain by itself is not capable of cortical association in the absence of a membrane targeting mechanism, it seems unlikely that the PA domain would bind directly to a multivalent membrane protein. Moreover, genome-wide screens of viable yeast deletion mutants have not been able to identify additional components in the dynein pathway that localize to the cell membrane (Tong et al., 2004; Lee et al., 2005). Therefore, evidence supporting this protein scaffold hypothesis is lacking.

An alternative mechanism by which Num1 decides where to assemble patches is by recognizing a specific feature or composition of the cell membrane through its BAR-like PA domain. BAR domains are highly elongated banana-shaped homodimers that bind preferentially to curved and negatively charged membranes (Farsad et al., 2001; Peter et al., 2004). We noted that the PA domain shares various features resembling a BAR domain: (a) it is located at the N terminus of Num1 (BAR domains are preferentially found at the N terminus of proteins; Henne et al., 2007; Shimada et al., 2007), (b) it has a high predicted helical content (95%; BAR domains are composed of mostly helices; Peter et al., 2004; Henne et al., 2007; Shimada et al., 2007; Ziółkowska et al., 2011), and (c) it is coupled with a PH domain (BAR domains are often paired with other membrane targeting modules, such as PH or PX domains, to synergistically localize proteins to membranes of specific composition and curvature; Peter et al., 2004). In addition, we experimentally showed that the PA domain exists as highly elongated dimers in solution, another feature similar to BAR domains. Furthermore, membrane-bound BAR dimers can further polymerize into helical coats that are held together by lateral and tip-to-tip interactions (Shimada et al., 2007; Frost et al., 2008; Karotki et al., 2011). The EK mutation within the PA domain of Num1, designed to

disrupt the tip-to-tip interaction between PA dimers, resulted in a significant loss of bright patches without disrupting dimerization (Figs. 7 [A–C] and S3 C), lending support to the structural similarity of the PA domain with BAR domains.

Interestingly, a recent study has implicated BAR domain–containing proteins in the organization of plasma membrane domains in budding yeast (Karotki et al., 2011). These proteins include Pil1 and Lsp1, which are able to self-assemble into scaffolds on the plasma membrane by binding to areas rich in $PI(4,5)P_2$ lipid (Karotki et al., 2011). Thus, it is tempting to speculate that Num1 patches represent membrane microdomains sculpted by its BAR-like PA domain. In Fig. 9, we propose a model illustrating the PA domain–mediated patch assembly pathway for cortical dynein anchoring. First, dimeric Num1 molecules are preferentially recruited to plasma membrane regions characterized by features recognized by its N-terminal PA domain (e.g., membrane furrows or small invaginations). Upon binding to the membrane, Num1 dimers further associate with each other to assemble into stationary patches at the cell cortex (Fig. 9 A). Membrane binding is mediated by a PH–$PI(4,5)P_2$ interaction, whereas the dimer–dimer association depends on the PA domain. Second, dynein associated with the plus end of astral microtubules interacts with cortical Num1 through the PA domain and becomes anchored at the cell cortex. Although dynein is able to bind Num1 patches of variable sizes, association with larger patches that anchor better to the membrane enables a stronger spindle-pulling force by dynein (Fig. 9 B). In this model, we hypothesize that dimeric Num1 assembles patches only at the cortex. However, it is possible that the Num1 complex may also be assembled in the cytoplasm, but these assemblies are unstable without being attached to the membrane. Future validation will await the crystal structure of the PA domain, which will verify its similarity to BAR domains and provide structural insights into dynein binding and activation at the cell cortex.

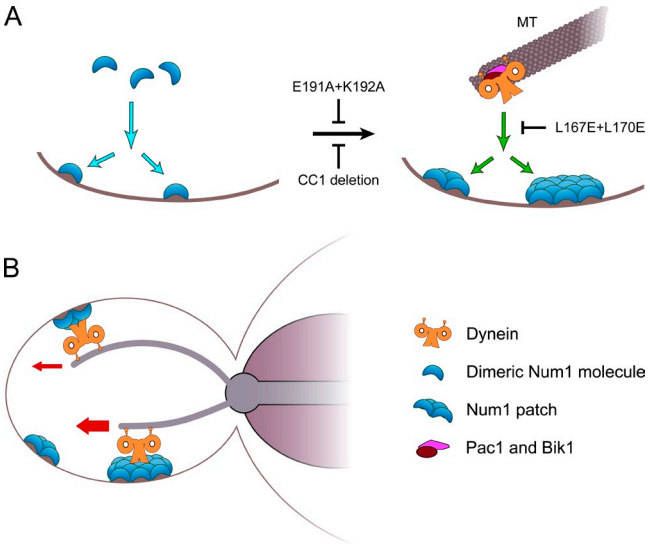

Figure 9. **Model for PA domain–mediated patch assembly and dynein anchoring.** (A, left) dimeric Num1 molecules are preferentially recruited to plasma membrane domains recognized by its N-terminal PA domain. Upon binding to the membrane, Num1 dimers further assemble into stationary patches through self-association. The dimer–dimer association of Num1 requires its PA domain and can be disrupted by the E191A + K192A mutation or by deleting the CC1 motif. On the other hand, the PH domain located at the C terminus of Num1 contributes to its membrane association by binding to membrane $PI(4,5)P_2$. (right) The dynein complex associated with the plus end of astral microtubules (MT) interacts with the membrane-bound Num1, thereby becoming anchored at the cell cortex. Interaction of Num1 with dynein is mediated by the PA domain and can be abolished by the L167E + L170E mutation located within the PA domain. (B) Dynein anchored to the Num1 patch pulls the nucleus and its associated spindle from the mother to the bud through the narrow bud neck. Although dynein is able to bind Num1 patches of variable sizes, anchoring to large patches enhances its activity and facilitates pulling of the spindle through the bud neck.

Materials and methods

Yeast strains and plasmids

All strains (Table S1) are isogenic with YWL36 (Vorvis et al., 2008) and were constructed by standard genetic cross- or PCR product–mediated transformation (Longtine et al., 1998). To generate deletion mutants of Num1 expressed from the endogenous chromosomal locus, we used the site-specific genomic mutagenesis approach (Gray et al., 2004). In brief, we amplified the *URA3* marker from pRS306 with F1 and R1 primers (Table S2) containing sequences flanking the targeted region and transformed the product into a Num1-GFP strain. We verified the substitution of the targeted sequence with *URA3* by diagnostic PCR from the genomic DNA. Next, we transformed the resulting strain with a PCR product containing an in-frame fusion of the sequences flanking the targeted region, amplified from wild-type genomic DNA using F2 and R2 primers (Table S2), along with a carrier plasmid containing the *LEU2* marker. Transformants were first selected for *LEU2* and then replica plated to media containing 5-fluoroorotic acid (5-FOA) to select against *URA3*. To construct point mutants of Num1, we generated a PCR fragment containing the mutated residues through an overlapping extension PCR procedure (Kanoksilapatham et al., 2007) with sequences for homologous recombination flanking each end of the PCR fragment. Next, we transformed the PCR fragment along with a carrier plasmid containing the *LEU2* marker into a yeast strain in which the corresponding chromosomal region has been replaced by a *URA3* marker. Transformants were first selected for *LEU2* and then replica plated to media containing 5-FOA to select for substitution of *URA3* with the PCR fragment. All point mutations were verified by DNA sequencing of the genomic locus.

Fusion of VC (aa 155–238 of Venus) to the N terminus of Num1 was constructed using the site-specific genomic approach, generating the *VC-NUM1* strain. To construct VC-$CC^{1–303}$, a PCR fragment encoding a stop codon followed by the *TRP1* marker was inserted after aa 303 of Num1 in the *VC-NUM1* strain, resulting in YWL3056. Fusion of VN (aa 1–172 of Venus) to the C terminus of Dyn1 was constructed by PCR product–mediated transformation using pRS303:*VN* as the PCR template (Markus et al., 2011).

To label microtubules, strains were transformed with pBJ1351 (*GFP-Tub1::LEU2*; Song and Lee, 2001), ApaI-digested pRS306-*MET3p:mCherry-TUB1* (*MET3p:mCherry-TUB1::URA3*; Markus et al., 2009), or StuI-digested pAFS125C (*CFP-TUB1::URA3*; Moore et al., 2008). Leu^+ or Ura^+ transformants were selected and examined for microtubule labeling by fluorescence microscopy.

To tag $CC^{1–303}$ and $CC^{1–325}$ with GFP-CAAX, HA, or Myc epitope, we performed PCR from the tagging vectors pKT0128-*RAS2*-C-term (Tang et al., 2009), pFA6a-3HA-TRP1, or pFA6a-13Myc-His3MX6 (Longtine et al., 1998), respectively, and integrated them into the chromosomal locus by transformation. Mitochondria were labeled with matrix-targeted Cox4-RFP using pHS78 (Cerveny et al., 2007). To construct GST-$CC^{1–325}$, a fragment containing aa 1–325 of Num1 was amplified from genomic DNA using a forward primer flanked with a BamHI site and a reverse primer flanked with a stop codon followed by an SalI site. The PCR fragment was digested with BamHI and SalI and ligated into similarly digested pGEX-KG, generating pXT55 that expresses GST-$CC^{1–325}$.

To construct the bacterial expression vector enabling purification using S-protein and IgG beads, a fragment containing Not1/PreScission site/S tag/Tobacco Etch Virus (TEV) site/IgG-binding motif (Z)/stop codon/KpnI was amplified from pKW804 (a gift from Y. Sun, University of California, San Francisco, San Francisco, CA). The PCR fragment was digested with NotI and KpnI and ligated into similarly digested pSY7 (a gift from R. Robinson, Institute of Molecular and Cell Biology, Singapore), generating pBSG01. A PCR fragment containing $CC^{95–303}$ was amplified

from genomic DNA using a forward primer flanked with an NcoI site and a reverse primer flanked with an NotI site, digested with NcoI and NotI, and ligated into similarly digested pBSG01, generating pBSG02 that expresses $CC^{95–303}$-S-TEV-Z.

Cell growth and microscopy

Cells for microscopy were cultured in synthetic defined media (Sunrise Science Products) at 30°C unless stated otherwise. Cells for total lysate preparations were cultured in YP (yeast extract and tryptone) media containing appropriate sugar (galactose or glucose). To induce the *GAL1* promoter, cells were cultured overnight in the presence of 2% raffinose, and then galactose was added to a final concentration of 2%. For cold nuclear segregation assay (Tang et al., 2009), early midlog culture at 30°C was shifted to 12°C for 16 h, fixed with 70% ethanol, and then stained with DAPI to visualize nuclei. To assay for spindle oscillation (Moore et al., 2009a), cells were cultured in synthetic defined media containing 200 mM HU for 2.5 h before imaging. To stain for cell boundary, cells were washed once with 10 mM Hepes plus 2% glucose and then incubated for 15 min in the same buffer containing 250 µM calcofluor. Subsequently, cells were either washed in synthetic defined media before microscopy or fixed in 4% formaldehyde for 30 min at room temperature and then washed with PBS before microscopy.

Widefield fluorescence images were collected at room temperature using a 1.49 NA 100× objective on an upright microscope (80i; Nikon) equipped with piezo-Z control (Physik Instrumente), electronically controlled SmartShutter (Sutter Instrument), motorized filter cube turret, and a cooled electron-multiplying charge-coupled device camera (Cascade II; Photometrics) controlled by NIS-Elements software (Nikon). Sputtered/ET filter cube sets (Chroma Technology Corp.) were used for imaging CFP (49001), GFP (49002), YFP (49003), and mCherry (49008) fluorescence. Confocal images were acquired using a 1.4 NA 100× objective on an inverted microscope (Ti-E; Nikon) equipped with a Revolution XD confocal system and 488/561-nm lasers (UMass Amherst Center for Biological Physics). Confocal z sections covering the entire cell were acquired with a step size of 0.1 µm. We used ImageJ (National Institutes of Health) to quantify fluorescence intensities of Num1 or Dyn1 foci (Markus et al., 2009).

Coimmunoprecipitation and in vitro pull-down assays

Coimmunoprecipitation of $CC^{1–325}$-3HA and $CC^{1–325}$-13Myc was performed using the Dynabeads Co-immunoprecipitation Kit (Invitrogen). In brief, cells were harvested, washed with distilled water, 20 mM Hepes, pH 7.5, and extraction buffer (immunoprecipitation buffer from the manufacturer with the addition of 100 mM NaCl, 0.2 mM DTT, and protease inhibitors). Cells were lysed in the exaction buffer by glass bead beating 4× 1 min using the Mini-Beadbeater (BioSpec Products). Cell debris was removed by centrifugation, and the supernatants were incubated with dynabeads coupled with anti-HA or -Myc antibody at 4°C for 30 min. Beads were washed, and bound proteins were eluted following the manufacturer's protocol for Western blot analysis. Rabbit polyclonal anti-HA antibody (Sigma-Aldrich) or mouse monoclonal anti-Myc antibody (9E10; Abcam) was used for immunoprecipitation. Rabbit polyclonal anti-HA (Sigma-Aldrich) and anti–c-Myc (GenScript) antibodies were used for Western blot analysis.

To purify GST-$CC^{1–325}$, BL21 Rosetta cells (EMD) carrying pXT55 were induced with 0.5 mM IPTG at 16°C for 15–17 h. Cells were harvested and lysed in protein extraction reagent (BugBuster; EMD) supplemented with protease inhibitors and Benzonase. After centrifugation, the supernatant was added to 400 µl GST resins (GST Bind kit, EMD) and incubated at room temperature for 30 min with gentle rotation followed by extensive wash with GST bind/wash buffer (4.3 mM Na_2HPO_4, 1.47 mM KH_2PO_4, 137 mM NaCl and 2.7 mM KCl, pH 7.3, and 1 mM PMSF). The resins were resuspended in ice-cold UB buffer (50 mM Hepes, pH 7.5, 100 mM KCl, 3 mM $MgCl_2$, 1 mM EGTA, 1 mM DTT, 1 mM PMSF, and protease inhibitors) before incubation with yeast lysate prepared from strains expressing either Pac11-13Myc or $Dyn1_{TAIL}$-3GFP. To prepare yeast lysate, midlog culture was harvested, washed with distilled water and UB buffer, and lysed in UB buffer by glass bead beating 4× 1 min using the Mini-Beadbeater. After centrifugation at 4°C for 25 min at 16,000 *g*, soluble supernatant was added to the resin-bound GST-$CC^{1–325}$ (prepared above) and incubated at 4°C for 30 min with gentle rotation. Resins were washed three times with high-salt UB buffer (50 mM Hepes, pH 7.5, 200 mM KCl, 3 mM $MgCl_2$, 1 mM EGTA, 1 mM DTT, 0.2% Tween 20, and 1mM PMSF). Bound proteins were eluted using GST elution buffer, precipitated by methanol/chloroform, and analyzed by SDS-PAGE followed by Western blotting.

To purify $CC^{95–303}$-S-Z, 500 ml BL21 Rosetta cells carrying pBSG02 was induced with 0.5 mM IPTG at 20°C for 15–17 h. Cells were harvested and resuspended in 4 ml IgG bind/wash buffer (150 mM NaCl, 20 mM Tris-Cl, pH 7.5, 0.05% Triton X-100, 1 mM EDTA, 1 mM DTT, and 1 mM PMSF) supplemented with protease inhibitor tablet (Roche) and lysed by vortexing in 1.5 ml of 0.1-mm glass beads for 5× 1 min using a benchtop vortex mixer. Cell lysates were cleared by centrifugation at 4°C for 20 min. The supernatant was added to 0.13 ml of S-protein agarose (EMD), incubated at 4°C for 45 min with gentle rocking, washed three times with IgG bind/wash buffer, and resuspended in 0.2 ml of UB buffer. Yeast cell lysate prepared as described above was then added to the S-protein agarose–bound $CC^{95–303}$-S-Z and incubated at 4°C for 30 min with gentle rotation. Resins were washed three times with high-salt UB buffer. Bound proteins were eluted by adding PreScission protease (releasing $CC^{95–303}$ from S-Z bound to beads) and incubating at 4°C for 2 h with gentle rotation. The eluate was precipitated by methanol/chloroform and analyzed by SDS-PAGE followed by Western blotting.

Analytical gel filtration and analytical ultracentrifugation

To purify $CC^{95–303}$-S for gel filtration, 4 liters of BL21 Rosetta cells carrying pBSG02 was induced with 0.5 mM IPTG at 20°C for 16 h. Harvested bacteria were resuspended in 64 ml of IgG bind/wash buffer supplemented with protease inhibitor tablet (Roche) and lysed by vortexing in 8 ml of 0.1-mm glass beads for 5× 1 min using a benchtop vortex mixer. Cell lysates were cleared by centrifugation at 4°C for 20 min. The supernatant was added to 1.5 ml of IgG Sepharose beads (GE Healthcare), incubated at 4°C for 45 min with gentle rocking, washed three times with IgG bind/wash buffer, resuspended in 1.2 ml of IgG bind/wash buffer containing TEV protease, and incubated at 16°C for 3 h with rotation. The TEV eluate ($CC^{95–303}$-S) was applied to a 200-ml Sephacryl S-200 column equilibrated with IgG bind/wash buffer. Fractions of 2 ml were collected and assayed by SDS-PAGE and Coomassie staining or by Western blotting with anti–S tag antibody. The S-200 column was calibrated with blue dextran (void volume), apoferritin (443 kD, *Rs* 6.1 nm), β-amylase (200 kD, *Rs* 5.40 nm), alcohol dehydrogenase (150 kD, *Rs* 4.6 nm), BSA (66 kD, *Rs* 3.55 nm), carbonic anhydrase (29 kD, *Rs* 2.36 nm), and ATP (salt volume). A Stokes radius of $CC^{95–303}$-S was obtained from the plot of $erfc^{-1}$ of the partition coefficients versus Stokes radius according to Ackers (1967).

Gel filtration fractions containing $CC^{95–303}$-S were pooled and concentrated (Amicon Ultra MWCO 3000; Millipore) to ∼0.6 mg/ml before analytical ultracentrifugation analysis. Sedimentation equilibrium was performed at 20°C using an An-60 Ti rotor in an ultracentrifuge (Optima XLI; Beckman Coulter; UMass Amherst Mass Spectrometry Center). We loaded $CC^{95–303}$-S, purified and gel filtered in IgG bind/wash buffer without Triton X-100 and with 0.1 mM *tris*(2-carboxyethyl)phosphine (instead of DTT), into two-sector Epon centerpieces and centrifuged them to equilibrium. We monitored absorption at 280 nm, collected datasets every hour, and used the HeteroAnalysis software (version 1.1.0.44; provided by J. Cole and J. Lary, University of Connecticut, Stamford, CT) to confirm the attainment of equilibrium and to determine the molecular mass of $CC^{95–303}$-S from the final datasets obtained at 20,000 and 28,000 rpm.

Online supplemental material

Fig. S1 shows localization and cold nuclear segregation phenotype of various *num1* mutants and an alignment of Num1 N-terminal sequences from *Saccharomyces cerevisiae*, *Candida glabrata*, and *Ashbya Gossypii*. Fig. S2 shows localization of Dyn1 or Jnm1, distribution of spindle velocity, and cold spindle orientation phenotype of the indicated *num1* mutants. Fig. S3 shows controls for the BiFC assay in Fig. 4 B, localization of overexpressed $CC^{1–325}$-GFP, and functional analysis of the $num1^{EK}$ mutant. Videos 1–5 show mitochondrial attachment to the cell cortex in *num1* mutants. Video 6 shows cortical mitochondrial attachment in $CC^{1–303}$-*PH dyn1Δ* and $CC^{1–303}$-*PH nip100Δ* cells. Video 7 shows cortical mitochondrial attachment in the $num1^{LL}$ mutant. Table S1 lists the yeast strains used in this study. Table S2 lists primer pairs used for constructing Num1 deletion mutants. Online supplemental material is available at http://www.jcb.org/cgi/content/full/jcb.201112017/DC1.

We wish to thank Dr. Stephen Eyles for generously offering the use of the XLI analytical ultracentrifuge housed in the UMass Mass Spectrometry Center. We would like to thank anonymous reviewers for their valuable suggestions to improve the manuscript. We thank Olivier Van Houtte for his help with measuring the intensity of Num1-GFP and Dyn1-3GFP foci using ImageJ. B. St. Germain was awarded a William and Margaret Nutting Scholarship.

This work was supported by a National Institutes of Health grant (R01GM076094) to W.-L. Lee.

Submitted: 5 December 2011
Accepted: 16 February 2012

References

Ackers, G.K. 1967. A new calibration procedure for gel filtration columns. *J. Biol. Chem.* 242:3237–3238.

Adames, N.R., and J.A. Cooper. 2000. Microtubule interactions with the cell cortex causing nuclear movements in *Saccharomyces cerevisiae*. *J. Cell Biol.* 149:863–874. http://dx.doi.org/10.1083/jcb.149.4.863

Bloom, K. 2001. Nuclear migration: Cortical anchors for cytoplasmic dynein. *Curr. Biol.* 11:R326–R329. http://dx.doi.org/10.1016/S0960-9822(01)00176-2

Blumer, J.B., R. Kuriyama, T.W. Gettys, and S.M. Lanier. 2006. The G-protein regulatory (GPR) motif-containing Leu-Gly-Asn-enriched protein (LGN) and Gialpha3 influence cortical positioning of the mitotic spindle poles at metaphase in symmetrically dividing mammalian cells. *Eur. J. Cell Biol.* 85:1233–1240. http://dx.doi.org/10.1016/j.ejcb.2006.08.002

Bowman, S.K., R.A. Neumüller, M. Novatchkova, Q. Du, and J.A. Knoblich. 2006. The *Drosophila* NuMA Homolog Mud regulates spindle orientation in asymmetric cell division. *Dev. Cell*. 10:731–742. http://dx.doi.org/10.1016/j.devcel.2006.05.005

Carminati, J.L., and T. Stearns. 1997. Microtubules orient the mitotic spindle in yeast through dynein-dependent interactions with the cell cortex. *J. Cell Biol.* 138:629–641. http://dx.doi.org/10.1083/jcb.138.3.629

Cerveny, K.L., S.L. Studer, R.E. Jensen, and H. Sesaki. 2007. Yeast mitochondrial division and distribution require the cortical num1 protein. *Dev. Cell*. 12:363–375. http://dx.doi.org/10.1016/j.devcel.2007.01.017

Chant, J., and J.R. Pringle. 1995. Patterns of bud-site selection in the yeast *Saccharomyces cerevisiae*. *J. Cell Biol.* 129:751–765. http://dx.doi.org/10.1083/jcb.129.3.751

Cole, J.L. 2004. Analysis of heterogeneous interactions. *Methods Enzymol.* 384:212–232. http://dx.doi.org/10.1016/S0076-6879(04)84013-8

Deschenes, R.J., and J.R. Broach. 1987. Fatty acylation is important but not essential for *Saccharomyces cerevisiae* RAS function. *Mol. Cell. Biol.* 7:2344–2351.

Du, Q., and I.G. Macara. 2004. Mammalian Pins is a conformational switch that links NuMA to heterotrimeric G proteins. *Cell*. 119:503–516. http://dx.doi.org/10.1016/j.cell.2004.10.028

Eshel, D., L.A. Urrestarazu, S. Vissers, J.C. Jauniaux, J.C. van Vliet-Reedijk, R.J. Planta, and I.R. Gibbons. 1993. Cytoplasmic dynein is required for normal nuclear segregation in yeast. *Proc. Natl. Acad. Sci. USA*. 90:11172–11176. http://dx.doi.org/10.1073/pnas.90.23.11172

Farkasovsky, M., and H. Küntzel. 1995. Yeast Num1p associates with the mother cell cortex during S/G2 phase and affects microtubular functions. *J. Cell Biol.* 131:1003–1014. http://dx.doi.org/10.1083/jcb.131.4.1003

Farkasovsky, M., and H. Küntzel. 2001. Cortical Num1p interacts with the dynein intermediate chain Pac11p and cytoplasmic microtubules in budding yeast. *J. Cell Biol.* 152:251–262. http://dx.doi.org/10.1083/jcb.152.2.251

Farsad, K., N. Ringstad, K. Takei, S.R. Floyd, K. Rose, and P. De Camilli. 2001. Generation of high curvature membranes mediated by direct endophilin bilayer interactions. *J. Cell Biol.* 155:193–200. http://dx.doi.org/10.1083/jcb.200107075

Faulkner, N.E., D.L. Dujardin, C.Y. Tai, K.T. Vaughan, C.B. O'Connell, Y. Wang, and R.B. Vallee. 2000. A role for the lissencephaly gene LIS1 in mitosis and cytoplasmic dynein function. *Nat. Cell Biol.* 2:784–791. http://dx.doi.org/10.1038/35041020

Finegold, A.A., W.R. Schafer, J. Rine, M. Whiteway, and F. Tamanoi. 1990. Common modifications of trimeric G proteins and ras protein: Involvement of polyisoprenylation. *Science*. 249:165–169. http://dx.doi.org/10.1126/science.1695391

Frost, A., R. Perera, A. Roux, K. Spasov, O. Destaing, E.H. Egelman, P. De Camilli, and V.M. Unger. 2008. Structural basis of membrane invagination by F-BAR domains. *Cell*. 132:807–817. http://dx.doi.org/10.1016/j.cell.2007.12.041

Geiser, J.R., E.J. Schott, T.J. Kingsbury, N.B. Cole, L.J. Totis, G. Bhattacharyya, L. He, and M.A. Hoyt. 1997. *Saccharomyces cerevisiae* genes required in the absence of the CIN8-encoded spindle motor act in functionally diverse mitotic pathways. *Mol. Biol. Cell*. 8:1035–1050.

Gray, M., M. Kupiec, and S.M. Honigberg. 2004. Site-specific genomic (SSG) and random domain-localized (RDL) mutagenesis in yeast. *BMC Biotechnol.* 4:7. http://dx.doi.org/10.1186/1472-6750-4-7

Hammermeister, M., K. Schödel, and B. Westermann. 2010. Mdm36 is a mitochondrial fission-promoting protein in *Saccharomyces cerevisiae*. *Mol. Biol. Cell*. 21:2443–2452. http://dx.doi.org/10.1091/mbc.E10-02-0096

Heil-Chapdelaine, R.A., J.R. Oberle, and J.A. Cooper. 2000. The cortical protein Num1p is essential for dynein-dependent interactions of microtubules with the cortex. *J. Cell Biol.* 151:1337–1344. http://dx.doi.org/10.1083/jcb.151.6.1337

Henne, W.M., H.M. Kent, M.G. Ford, B.G. Hegde, O. Daumke, P.J. Butler, R. Mittal, R. Langen, P.R. Evans, and H.T. McMahon. 2007. Structure and analysis of FCHo2 F-BAR domain: A dimerizing and membrane recruitment module that effects membrane curvature. *Structure*. 15:839–852. http://dx.doi.org/10.1016/j.str.2007.05.002

Howell, B.J., B.F. McEwen, J.C. Canman, D.B. Hoffman, E.M. Farrar, C.L. Rieder, and E.D. Salmon. 2001. Cytoplasmic dynein/dynactin drives kinetochore protein transport to the spindle poles and has a role in mitotic spindle checkpoint inactivation. *J. Cell Biol.* 155:1159–1172. http://dx.doi.org/10.1083/jcb.200105093

Itoh, T., K.S. Erdmann, A. Roux, B. Habermann, H. Werner, and P. De Camilli. 2005. Dynamin and the actin cytoskeleton cooperatively regulate plasma membrane invagination by BAR and F-BAR proteins. *Dev. Cell*. 9:791–804. http://dx.doi.org/10.1016/j.devcel.2005.11.005

Izumi, Y., N. Ohta, K. Hisata, T. Raabe, and F. Matsuzaki. 2006. *Drosophila* Pins-binding protein Mud regulates spindle-polarity coupling and centrosome organization. *Nat. Cell Biol.* 8:586–593. http://dx.doi.org/10.1038/ncb1409

Johnston, C.A., K. Hirono, K.E. Prehoda, and C.Q. Doe. 2009. Identification of an Aurora-A/PinsLINKER/Dlg spindle orientation pathway using induced cell polarity in S2 cells. *Cell*. 138:1150–1163. http://dx.doi.org/10.1016/j.cell.2009.07.041

Kahana, J.A., G. Schlenstedt, D.M. Evanchuk, J.R. Geiser, M.A. Hoyt, and P.A. Silver. 1998. The yeast dynactin complex is involved in partitioning the mitotic spindle between mother and daughter cells during anaphase B. *Mol. Biol. Cell*. 9:1741–1756.

Kanoksilapatham W, J.M. González, and F.T. Robb. 2007. Directed-mutagenesis and deletion generated through an improved overlapping-extension PCR based procedure. *Silpakorn U. Science & Tech. J.* 1:7–12.

Karotki, L., J.T. Huiskonen, C.J. Stefan, N.E. Ziółkowska, R. Roth, M.A. Surma, N.J. Krogan, S.D. Emr, J. Heuser, K. Grünewald, and T.C. Walther. 2011. Eisosome proteins assemble into a membrane scaffold. *J. Cell Biol.* 195:889–902. http://dx.doi.org/10.1083/jcb.201104040

Lee, W.L., J.R. Oberle, and J.A. Cooper. 2003. The role of the lissencephaly protein Pac1 during nuclear migration in budding yeast. *J. Cell Biol.* 160:355–364. http://dx.doi.org/10.1083/jcb.200209022

Lee, W.L., M.A. Kaiser, and J.A. Cooper. 2005. The offloading model for dynein function: Differential function of motor subunits. *J. Cell Biol.* 168:201–207. http://dx.doi.org/10.1083/jcb.200407036

Li, Y.Y., E. Yeh, T. Hays, and K. Bloom. 1993. Disruption of mitotic spindle orientation in a yeast dynein mutant. *Proc. Natl. Acad. Sci. USA*. 90:10096–10100. http://dx.doi.org/10.1073/pnas.90.21.10096

Longtine, M.S., A. McKenzie III, D.J. Demarini, N.G. Shah, A. Wach, A. Brachat, P. Philippsen, and J.R. Pringle. 1998. Additional modules for versatile and economical PCR-based gene deletion and modification in *Saccharomyces cerevisiae*. *Yeast*. 14:953–961.

Markus, S.M., and W.L. Lee. 2011a. Microtubule-dependent path to the cell cortex for cytoplasmic dynein in mitotic spindle orientation. *BioArchitecture*. 1:1–7. http://dx.doi.org/10.4161/bioa.1.1.15419

Markus, S.M., and W.L. Lee. 2011b. Regulated offloading of cytoplasmic dynein from microtubule plus ends to the cortex. *Dev. Cell*. 20:639–651. http://dx.doi.org/10.1016/j.devcel.2011.04.011

Markus, S.M., J.J. Punch, and W.L. Lee. 2009. Motor- and tail-dependent targeting of dynein to microtubule plus ends and the cell cortex. *Curr. Biol.* 19:196–205. http://dx.doi.org/10.1016/j.cub.2008.12.047

Markus, S.M., K.M. Plevock, B.J. St Germain, J.J. Punch, C.W. Meaden, and W.L. Lee. 2011. Quantitative analysis of Pac1/LIS1-mediated dynein targeting: Implications for regulation of dynein activity in budding yeast. *Cytoskeleton (Hoboken)*. 68:157–174.

McMillan, J.N., and K. Tatchell. 1994. The JNM1 gene in the yeast *Saccharomyces cerevisiae* is required for nuclear migration and spindle orientation during the mitotic cell cycle. *J. Cell Biol.* 125:143–158. http://dx.doi.org/10.1083/jcb.125.1.143

Mendoza, M., C. Norden, K. Durrer, H. Rauter, F. Uhlmann, and Y. Barral. 2009. A mechanism for chromosome segregation sensing by the NoCut checkpoint. *Nat. Cell Biol.* 11:477–483. http://dx.doi.org/10.1038/ncb1855

Merdes, A., R. Heald, K. Samejima, W.C. Earnshaw, and D.W. Cleveland. 2000. Formation of spindle poles by dynein/dynactin-dependent transport of NuMA. *J. Cell Biol.* 149:851–862. http://dx.doi.org/10.1083/jcb.149.4.851

Miller, R.K., and M.D. Rose. 1998. Kar9p is a novel cortical protein required for cytoplasmic microtubule orientation in yeast. *J. Cell Biol.* 140:377–390. http://dx.doi.org/10.1083/jcb.140.2.377

Miller, R.K., D. Matheos, and M.D. Rose. 1999. The cortical localization of the microtubule orientation protein, Kar9p, is dependent upon actin and proteins required for polarization. *J. Cell Biol.* 144:963–975. http://dx.doi.org/10.1083/jcb.144.5.963

Moore, J.K., J. Li, and J.A. Cooper. 2008. Dynactin function in mitotic spindle positioning. *Traffic*. 9:510–527. http://dx.doi.org/10.1111/j.1600-0854.2008.00710.x

Moore, J.K., D. Sept, and J.A. Cooper. 2009a. Neurodegeneration mutations in dynactin impair dynein-dependent nuclear migration. *Proc. Natl. Acad. Sci. USA*. 106:5147–5152. http://dx.doi.org/10.1073/pnas.0810828106

Moore, J.K., M.D. Stuchell-Brereton, and J.A. Cooper. 2009b. Function of dynein in budding yeast: Mitotic spindle positioning in a polarized cell. *Cell Motil. Cytoskeleton*. 66:546–555. http://dx.doi.org/10.1002/cm.20364

Nguyen-Ngoc, T., K. Afshar, and P. Gönczy. 2007. Coupling of cortical dynein and G alpha proteins mediates spindle positioning in *Caenorhabditis elegans*. *Nat. Cell Biol.* 9:1294–1302. http://dx.doi.org/10.1038/ncb1649

Peter, B.J., H.M. Kent, I.G. Mills, Y. Vallis, P.J. Butler, P.R. Evans, and H.T. McMahon. 2004. BAR domains as sensors of membrane curvature: The amphiphysin BAR structure. *Science*. 303:495–499. http://dx.doi.org/10.1126/science.1092586

Poulson, N.D., and T. Lechler. 2010. Robust control of mitotic spindle orientation in the developing epidermis. *J. Cell Biol.* 191:915–922. http://dx.doi.org/10.1083/jcb.201008001

Pringle, J.R., E. Bi, H.A. Harkins, J.E. Zahner, C. De Virgilio, J. Chant, K. Corrado, and H. Fares. 1995. Establishment of cell polarity in yeast. *Cold Spring Harb. Symp. Quant. Biol.* 60:729–744. http://dx.doi.org/10.1101/SQB.1995.060.01.079

Quintyne, N.J., J.E. Reing, D.R. Hoffelder, S.M. Gollin, and W.S. Saunders. 2005. Spindle multipolarity is prevented by centrosomal clustering. *Science*. 307:127–129. http://dx.doi.org/10.1126/science.1104905

Roy, A., A. Kucukural, and Y. Zhang. 2010. I-TASSER: A unified platform for automated protein structure and function prediction. *Nat. Protoc.* 5:725–738. http://dx.doi.org/10.1038/nprot.2010.5

Saito, T.T., D. Okuzaki, and H. Nojima. 2006. Mcp5, a meiotic cell cortex protein, is required for nuclear movement mediated by dynein and microtubules in fission yeast. *J. Cell Biol.* 173:27–33. http://dx.doi.org/10.1083/jcb.200512129

Salina, D., K. Bodoor, D.M. Eckley, T.A. Schroer, J.B. Rattner, and B. Burke. 2002. Cytoplasmic dynein as a facilitator of nuclear envelope breakdown. *Cell*. 108:97–107. http://dx.doi.org/10.1016/S0092-8674(01)00628-6

Ségalen, M., C.A. Johnston, C.A. Martin, J.G. Dumortier, K.E. Prehoda, N.B. David, C.Q. Doe, and Y. Bellaïche. 2010. The Fz-Dsh planar cell polarity pathway induces oriented cell division via Mud/NuMA in *Drosophila* and zebrafish. *Dev. Cell*. 19:740–752. http://dx.doi.org/10.1016/j.devcel.2010.10.004

Shaw, S.L., E. Yeh, P. Maddox, E.D. Salmon, and K. Bloom. 1997. Astral microtubule dynamics in yeast: A microtubule-based searching mechanism for spindle orientation and nuclear migration into the bud. *J. Cell Biol.* 139:985–994. http://dx.doi.org/10.1083/jcb.139.4.985

Sheeman, B., P. Carvalho, I. Sagot, J. Geiser, D. Kho, M.A. Hoyt, and D. Pellman. 2003. Determinants of *S. cerevisiae* dynein localization and activation: Implications for the mechanism of spindle positioning. *Curr. Biol.* 13:364–372. http://dx.doi.org/10.1016/S0960-9822(03)00013-7

Shimada, A., H. Niwa, K. Tsujita, S. Suetsugu, K. Nitta, K. Hanawa-Suetsugu, R. Akasaka, Y. Nishino, M. Toyama, L. Chen, et al. 2007. Curved EFC/F-BAR-domain dimers are joined end to end into a filament for membrane invagination in endocytosis. *Cell*. 129:761–772. http://dx.doi.org/10.1016/j.cell.2007.03.040

Shyu, Y.J., S.M. Hiatt, H.M. Duren, R.E. Ellis, T.K. Kerppola, and C.D. Hu. 2008. Visualization of protein interactions in living *Caenorhabditis elegans* using bimolecular fluorescence complementation analysis. *Nat. Protoc.* 3:588–596. http://dx.doi.org/10.1038/nprot.2008.16

Siller, K.H., and C.Q. Doe. 2009. Spindle orientation during asymmetric cell division. *Nat. Cell Biol.* 11:365–374. http://dx.doi.org/10.1038/ncb0409-365

Siller, K.H., C. Cabernard, and C.Q. Doe. 2006. The NuMA-related Mud protein binds Pins and regulates spindle orientation in *Drosophila* neuroblasts. *Nat. Cell Biol.* 8:594–600. http://dx.doi.org/10.1038/ncb1412

Song, S., and K.S. Lee. 2001. A novel function of *Saccharomyces cerevisiae CDC5* in cytokinesis. *J. Cell Biol.* 152:451–469. http://dx.doi.org/10.1083/jcb.152.3.451

Srinivasa, S.P., L.S. Bernstein, K.J. Blumer, and M.E. Linder. 1998. Plasma membrane localization is required for RGS4 function in *Saccharomyces cerevisiae*. *Proc. Natl. Acad. Sci. USA*. 95:5584–5589. http://dx.doi.org/10.1073/pnas.95.10.5584

Stearns, T. 1997. Motoring to the finish: Kinesin and dynein work together to orient the yeast mitotic spindle. *J. Cell Biol.* 138:957–960. http://dx.doi.org/10.1083/jcb.138.5.957

Stuchell-Brereton, M.D., A. Siglin, J. Li, J.K. Moore, S. Ahmed, J.C. Williams, and J.A. Cooper. 2011. Functional interaction between dynein light chain and intermediate chain is required for mitotic spindle positioning. *Mol. Biol. Cell*. 22:2690–2701. http://dx.doi.org/10.1091/mbc.E11-01-0075

Sullivan, D.S., and T.C. Huffaker. 1992. Astral microtubules are not required for anaphase B in *Saccharomyces cerevisiae*. *J. Cell Biol.* 119:379–388. http://dx.doi.org/10.1083/jcb.119.2.379

Tang, X., J.J. Punch, and W.L. Lee. 2009. A CAAX motif can compensate for the PH domain of Num1 for cortical dynein attachment. *Cell Cycle*. 8:3182–3190. http://dx.doi.org/10.4161/cc.8.19.9731

Tong, A.H., G. Lesage, G.D. Bader, H. Ding, H. Xu, X. Xin, J. Young, G.F. Berriz, R.L. Brost, M. Chang, et al. 2004. Global mapping of the yeast genetic interaction network. *Science*. 303:808–813. http://dx.doi.org/10.1126/science.1091317

Vorvis, C., S.M. Markus, and W.L. Lee. 2008. Photoactivatable GFP tagging cassettes for protein-tracking studies in the budding yeast *Saccharomyces cerevisiae*. *Yeast*. 25:651–659. http://dx.doi.org/10.1002/yea.1611

Wang, Q., M.V. Navarro, G. Peng, E. Molinelli, S.L. Goh, B.L. Judson, K.R. Rajashankar, and H. Sondermann. 2009. Molecular mechanism of membrane constriction and tubulation mediated by the F-BAR protein Pacsin/Syndapin. *Proc. Natl. Acad. Sci. USA*. 106:12700–12705. http://dx.doi.org/10.1073/pnas.0902974106

Williams, S.E., S. Beronja, H.A. Pasolli, and E. Fuchs. 2011. Asymmetric cell divisions promote Notch-dependent epidermal differentiation. *Nature*. 470:353–358. http://dx.doi.org/10.1038/nature09793

Wojcik, E., R. Basto, M. Serr, F. Scaërou, R. Karess, and T. Hays. 2001. Kinetochore dynein: Its dynamics and role in the transport of the Rough deal checkpoint protein. *Nat. Cell Biol.* 3:1001–1007. http://dx.doi.org/10.1038/ncb1101-1001

Woodard, G.E., N.N. Huang, H. Cho, T. Miki, G.G. Tall, and J.H. Kehrl. 2010. Ric-8A and Gi alpha recruit LGN, NuMA, and dynein to the cell cortex to help orient the mitotic spindle. *Mol. Cell. Biol.* 30:3519–3530. http://dx.doi.org/10.1128/MCB.00394-10

Yamashita, A., and M. Yamamoto. 2006. Fission yeast Num1p is a cortical factor anchoring dynein and is essential for the horse-tail nuclear movement during meiotic prophase. *Genetics*. 173:1187–1196. http://dx.doi.org/10.1534/genetics.105.050062

Yeh, E., R.V. Skibbens, J.W. Cheng, E.D. Salmon, and K. Bloom. 1995. Spindle dynamics and cell cycle regulation of dynein in the budding yeast, *Saccharomyces cerevisiae*. *J. Cell Biol.* 130:687–700. http://dx.doi.org/10.1083/jcb.130.3.687

Yeh, E., C. Yang, E. Chin, P. Maddox, E.D. Salmon, D.J. Lew, and K. Bloom. 2000. Dynamic positioning of mitotic spindles in yeast: Role of microtubule motors and cortical determinants. *Mol. Biol. Cell*. 11:3949–3961.

Yin, H., D. Pruyne, T.C. Huffaker, and A. Bretscher. 2000. Myosin V orientates the mitotic spindle in yeast. *Nature*. 406:1013–1015. http://dx.doi.org/10.1038/35023024

Yu, J.W., J.M. Mendrola, A. Audhya, S. Singh, D. Keleti, D.B. DeWald, D. Murray, S.D. Emr, and M.A. Lemmon. 2004. Genome-wide analysis of membrane targeting by *S. cerevisiae* pleckstrin homology domains. *Mol. Cell*. 13:677–688. http://dx.doi.org/10.1016/S1097-2765(04)00083-8

Ziółkowska, N.E., L. Karotki, M. Rehman, J.T. Huiskonen, and T.C. Walther. 2011. Eisosome-driven plasma membrane organization is mediated by BAR domains. *Nat. Struct. Mol. Biol.* 18:854–856. http://dx.doi.org/10.1038/nsmb.2080